Sensors and Materials, Vol. 36, No. 3 (2024) 989–1001
MYU Tokyo

S & M 3576

Detection of Elevator Cable Slippage Using Streaming Image Process Algorithm

Hsiung-Cheng Lin* and Yan-Hao Peng

Department of Electronic Engineering, National Chin-Yi University of Technology
No. 57, Sec. 2, Zhongshan Rd., Taiping Dist., Taichung 411030, Taiwan

(Received October 2, 2023; accepted February 15, 2024)

Keywords: elevator, main wheel, cable, slippage, image

Elevators are the most common transportation tool in modern buildings. To satisfy the safety requirement, it is mandatory to carry out regular maintenance in a certain period of time. Among maintenance items, the determination of the traction compartment cable slippage status is one of the greatest challenges in the elevator industry, but a simple and effective method is still lacking. Currently, in a real situation, the inspection accuracy relies considerably on suitable personnel experiences, and the inspection process is also time-consuming. Accordingly, we aim to develop an automatic streaming image process model for the detection of the elevator cable slipping distance. First, the geometric shape of an ellipse is established from a captured circle image. Second, the ellipse is averaged and segmented into 360° with a predefined label as a reference point. Third, the circumference formula is applied to the calculation of the cable slipping distance. Finally, the outcome of the arithmetic operation is sent to the cloud database through a graphical user interface (GUI) on the web for monitoring purposes. The experimental results reveal that the standard deviation is as small as 1.153 mm, and the measurement uncertainty is only 0.258 mm, demonstrating high accuracy, rapidity, and robustness.

1. Introduction

In elevators, wire cables are largely used to support the cage and the compensation cable, which is connected to the compensation sheave. They usually are subject to considerable loads and thus always suffer tremendous mechanical damage during their service life.[1–5] Research on elevator cables has verified that the major risk during elevator operation may arise from cable slippage. Sometimes damage may be easily detected by visual inspection, while in most other cases, fractured wires may be hidden on the inside.[6–9] To ensure the safety of elevator operation, International Standard ISO4101 was developed by Technical Committee ISO/TC 105, Steel Wire Ropes, and circulated to member bodies in October 1982.[10] Regular inspections are therefore mandatory to ensure a high level of safety for both personnel and equipment during elevator operation. According to this standard, the elevator cable is required to be replaced under any one of the following conditions: 1. more than 10% of the steel wire is fractured; 2. the rope

*Corresponding author: e-mail: hclin@ncut.edu.tw
https://doi.org/10.18494/SAM4677

ISSN 0914-4935
https://myukk.org/

has become thin with a diameter 7% less than the original size; 3. distortion exists; 4. rust erosion has occurred. These problems usually accompany cable slippage, which is the most important index for evaluating elevator safety.[11–13]

The shortening of the life of multicable elevators as a result of problems such as vibration, noise, uneven wear of key components, and uneven distribution of rope tension is still unclarified in the elevator industry. Accordingly, the theoretical modeling of the coupled vibrations of the building and elevator cables has been reported.[14–16] It was indicated that the elevator cable is a flexible wire with low damping, so it is prone to vibrations. In the case of a high-rise building, the large rope length may have a high possibility of resonance. In addition, an investigation on the vibration of elevator cables in a high-rise elevator system under earthquake excitation has been presented.[17] In this study, various cable lengths that may cause natural resonance and the effect of time-variant variables on the damping ratio were considered. The dynamics of the cables were also analyzed and solved numerically using the governing nonstationary, nonlinear equation. To reduce the vibrations caused by the resonance of the elevator cable owing to building sway, the vibration control approach of using a nonstationary robust control method was proposed.[18] Although several methods of estimating the vibration displacement using image processing or laser displacement meters with an observer or a Kalan filter were developed, observing the vibration of the elevator cables in an elevator shaft is a difficult task because of the movement of the elevator car and the thinness of the cable as an observation target.[19]

More importantly, the metal fatigue, along with abrasion, of the elevator cable may lead to the progressive loss of the metallic cross section.[20,21] Some features such as the roughened and pitted surfaces of the cables, reduced cable diameter, and broken wires can be seen. Therefore, the deterioration must be monitored before any unexpected damage or corrosion causes a fatal accident.[22] Ultrasound-guided wave-based inspection can be applied to monitor the cross section of wire cables. However, its efficacy in detecting defects in wire cables is low. For this reason, the finite element analysis of dispersion curves was conducted to study guided wave propagation in wire cables.[23] Recently, a new method of detecting broken steel wires on the cable surface using the conducting property of the cable has been reported.[24] It revealed that the spiral cable characteristic affects the eddy current response signal in the broken wires. On the basis of this principle, an eddy current differential probe was designed to improve the detection accuracy in a simulation. However, its applicability in practice is not yet confirmed. To balance the different tensions and the axial deformation of each cable, automatic balance equipment for cable-type elevators was proposed.[25] The results of using the Simscape numerical methodology showed that the imbalance rate of the system could be effectively limited to a low level.

2. System Structure

The proposed system structure is shown in Fig. 1. The main procedure is as follows. (1) A video of the elevator-cable main wheel operation is taken using an IP camera (IP Cam). (2) The collected image plus the elevator ID number and detection date with time are then sent to the dynamic image measuring model via Transmission Control Protocol/Internet Protocol (TCP/IP)

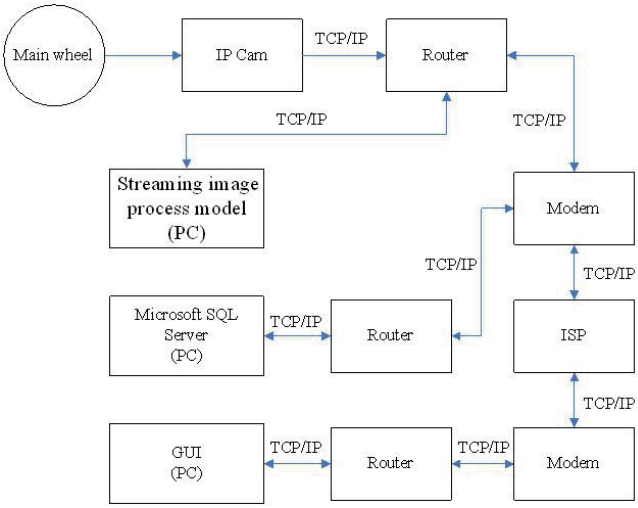

Fig. 1. (Color online) System structure.

using a router for further calculation. (3) The calculation results obtained using the proposed model are transmitted to a Microsoft SQL Server through the modem and router using TCP/IP. (4) The cable slipping distance data can be read by the graphical user interface (GUI) via the modem, ISP, and router.

(1) IP Cam: It is used to transform the detected image into a video stream to be processed via TCP/IP by the computer.
(2) Dynamic image measuring model: The slipping distance of the elevator cable is calculated on the basis of the video stream collected from the IP Cam.
(3) Microsoft SQL Server: The cloud database is used to save the elevator ID number, detection date and time, cable slipping distance, and so forth. Simultaneously, it can provide an IP address for a remote authorized client (PC) to access the server.
(4) GUI: It provides a friendly operation interface for reading the cable slipping information as well as defining the abnormal cable situation.

3. Proposed Model

3.1 Model principle

The practical elevator cable main wheel is a circle, as shown in Fig. 2. The circle is used to derive the mathematical equation for the proposed model.[26]

In Fig. 3, an arbitrary point $P(r\cos\theta, r\sin\theta)$ on the circle to the center of the circle, $O(0, 0)$, is a constant radius, r, where the angle with the x-axis is θ ($0 \leq \theta < 2\pi$), and the perimeter $l = r\theta$. Therefore, the circle equation is formed as $x^2 + y^2 = r^2$, where $x = r\cos\theta$ and $y = r\sin\theta$.

When a photograph of the main wheel is taken, the image will become an elliptical shape as shown in Fig. 4. Assume $P(x, y)$ is an arbitrary ellipse point, where $F_1(c, 0)$ and $F_2(-c, 0)$ are two points of focus, O is a center point, a is the semi-major axis, b is the semi-minor axis, c is the semi-focus point, and p is the half-sinusoid.

Fig. 2. (Color online) Elevator cable main wheel.

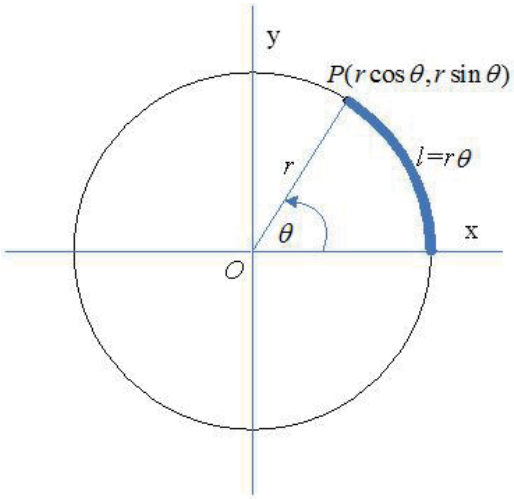

Fig. 3. (Color online) Schematic diagram of circle coordinates.

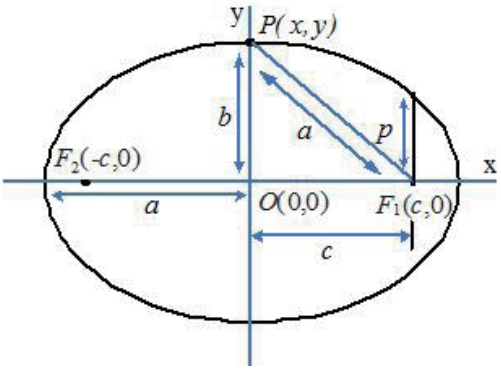

Fig. 4. (Color online) Ellipse coordinates.

The ellipse trajectory equation is defined as

$$|PF_1| + |PF_2| = 2a, \tag{1}$$

where $2a$ is a constant length.

As shown in Fig. 5, the ellipse equation is $\frac{x^2}{a^2} + \frac{y^2}{b^2} = 1$, $a > b > 0$, if the focus is located on the x-axis. On the other hand, it is $\frac{y^2}{a^2} + \frac{x^2}{b^2} = 1$, where $a > b > 0$ and $a^2 - b^2 = c^2$, if the focus is located on the y-axis.

3.2 Proposed model

Initially, the circle is equally divided into 360°, as shown in Fig. 6. Its respective ellipse is shown in Fig. 7, where a red label (A) marks the reference point for the wheel rotation phase.

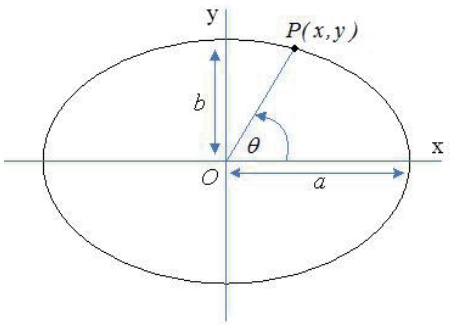

Fig. 5. (Color online) Profile of ellipse semi-major and semi-minor axes.

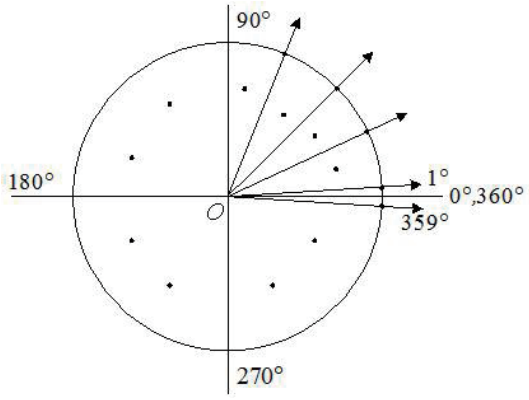

Fig. 6. Profile of circle with equal divisions of 360°.[26]

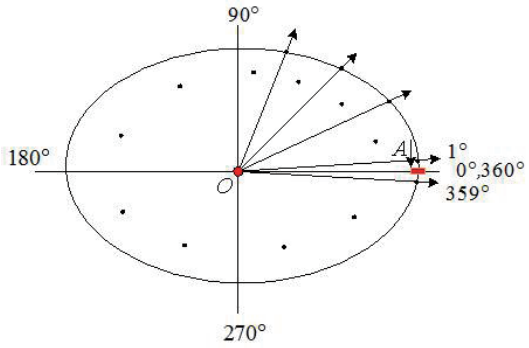

Fig. 7. (Color online) Profile of equal divisions of 360°.[26]

Because of a slipping phenomenon, the A point is expected to exceed θ degree from the original location of 0°, as shown in Fig. 8. The number of rotations of the main wheel is N under a normal operation, where N is the standard number of rotations for the elevator car to travel from the highest level to the lowest level. The actual number of rotations is designated as M. In practice, $M \geq N$, where M and N are integers.

The total cable slipping distance (L) can be calculated as[26]

$$L = (M - N) \times 2\pi r + r\theta, \tag{2}$$

where r is the main wheel radius and θ is the excess slipping angle.

4. Model Process

The proposed model process flowchart is shown in Fig. 9, and its major process is briefly described below.

(1) Take a video of the main wheel.
(2) Implement Gaussian blur processing.

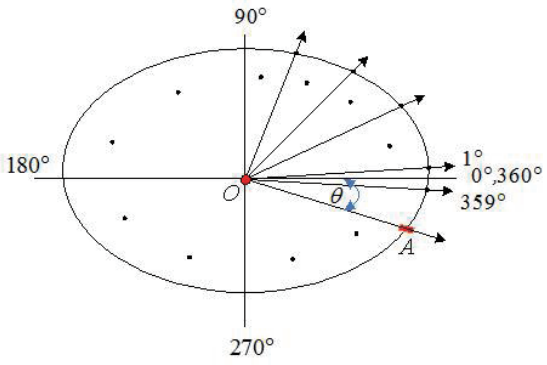

Fig. 8. (Color online) Ellipse profile of excessive rotating degree θ.[26]

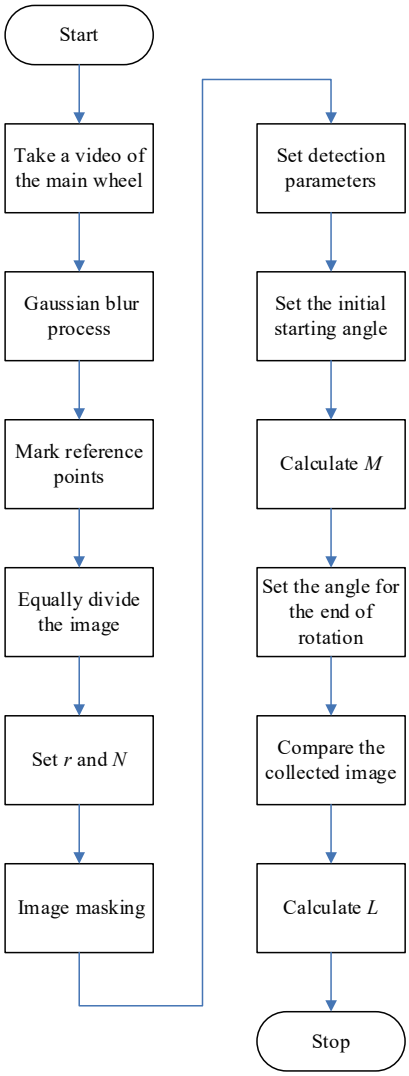

Fig. 9. (Color online) Flowchart of model process.

(3) Mark Up, Down, Left, Right, and Center reference points.
(4) Equally divide the image into 360° to create the standard ellipse image.
(5) Set the main wheel radius r and the standard number of rotations, N.
(6) Perform image masking.
(7) Set detection parameters.
(8) Set the initial starting angle.
(9) Calculate the number of rotations, M.
(10) Set the angle for the end of rotation.
(11) Compare the collected image with the standard image once the main wheel stops.
(12) Calculate $L = (M - N) \times 2\pi r + r\theta$.

5. Dynamic Image Processing with Experimental Results

In this study, one surveillance IP Cam installed in front of the main wheel was used. The resolution of the surveillance IP Cam is 1920 ×1080 pixel, and the frame rate is 30 frames per second with the baud rate of 4096 kbps for image transmission.

5.1 Dynamic image processing

The main wheel image is shown in Fig. 10, where the black label indicates the reference point.

The main procedure to implement the proposed model is demonstrated as follows.

(1) Enter the main operation panel, as shown in Fig. 11.
(2) Path: Set the real-time streaming protocol (RTSP) address, as shown in Fig. 12.
(3) Connect: Connect to the dedicated IP address by clicking the "Connect" button, as shown in Fig. 13.
(4) Play: Play the video of the rotating main wheel, as shown in Fig. 14.
(5) Flip: Flip the image, as shown in Fig. 15.
(6) Point: Display the reference point of the image, as shown in Fig. 16.
(7) Select the center reference point with pixel coordinates x: 501, y: 405, as shown in Fig. 17.
(8) Auxiliary Line: Set the auxiliary line for Up, Down, Left, and Right (vertical or parallel mode), as shown in Fig. 18.
(9) Select the Up reference point with pixel coordinates x: 501, y: 235, as shown in Fig. 19.
(10) Select the Down reference point with pixel coordinates x: 501, y: 574, as shown in Fig. 20.
(11) Select the Left reference point with pixel coordinates x: 375, y: 405, as shown in Fig. 21.
(12) Select the Right reference point with pixel coordinates x: 629, y: 405, as shown in Fig. 22.
(13) Close the auxiliary line, as shown in Fig. 23.
(14) Set the start and end angles to calculate the number of main wheel rotations, as shown in Fig. 24.
(15) Process Gaussian blur to reduce image noise, as shown in Fig. 25.
(16) Implement the mask function, as shown in Fig. 26.
(17) Start the detection process, as shown in Fig. 27.

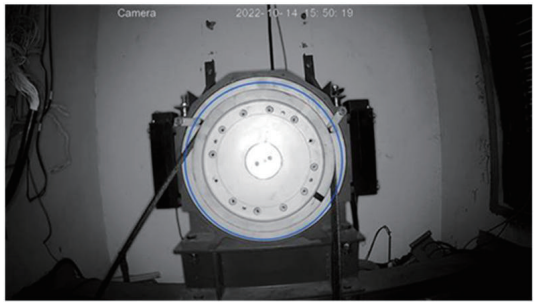

Fig. 10. (Color online) Main wheel image.[26]

Fig. 11. (Color online) Main operation panel.

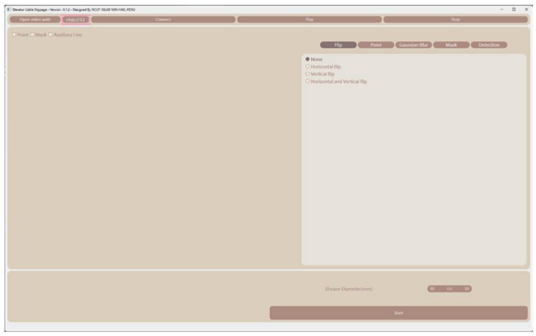

Fig. 12. (Color online) Setting the RTSP address.

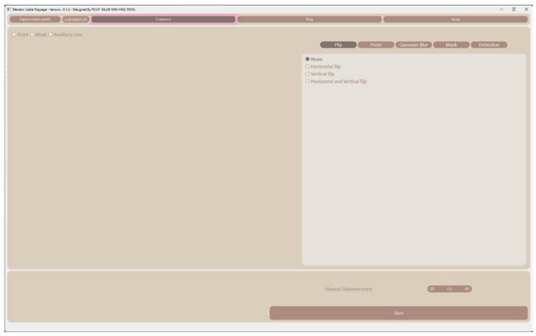

Fig. 13. (Color online) Dedicated IP address.

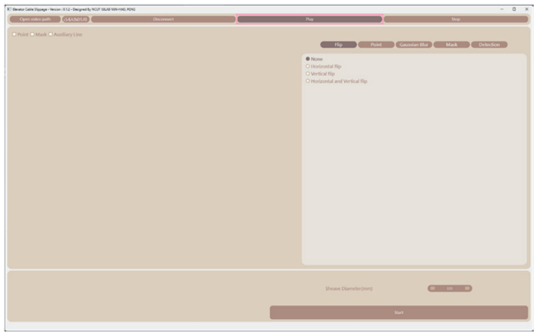

Fig. 14. (Color online) Video of rotating main wheel.

Fig. 15. (Color online) Flipping the image.

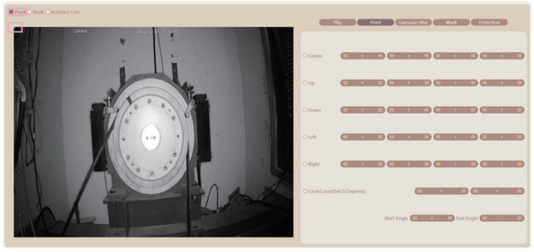

Fig. 16. (Color online) Reference point.

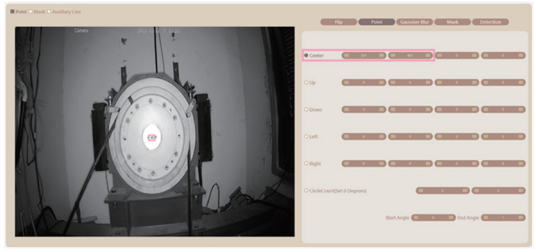

Fig. 17. (Color online) Center reference point.

Fig. 18. (Color online) Action of auxiliary lines.

Fig. 19. (Color online) Up reference point.

Fig. 20. (Color online) Down reference point.

Fig. 21. (Color online) Left reference point.

Fig. 22. (Color online) Right reference point.

Fig. 23. (Color online) End of auxiliary lines.

Fig. 24. (Color online) Setting start and end angles.

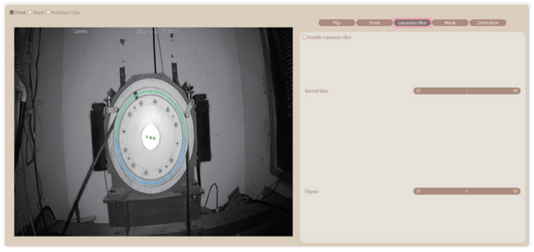

Fig. 25. (Color online) Implementation of Gaussian blur processing.

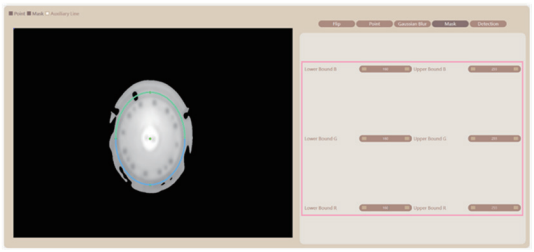

Fig. 26. (Color online) Implementing mask function.

Fig. 27. (Color online) Outline of detection process.

(18) The location of the start angle is marked A in Fig. 28, where its value is 110.5°, as shown in the pink frame at the bottom of the figure. The elevator starts to operate from the start angle.
(19) The location of the end angle is marked B in Fig. 29 when the elevator stops. Its value of 101.0°, is seen in the pink frame at the bottom of the figure. From Eq. (1), the slipping distance is obtained as 26.529 mm. Note that the number of main wheel clockwise (CS) rotations, i.e., 24, is the same as that of main wheel counterclockwise (CCS) rotations, as shown in the pink frame at the bottom left in the figure.

5.2 Experimental results

Twenty tests were carried out for the elevator operation of a round trip between the first floor and the fourth floor, which is at a height of about 12 m. Microsoft SQL Server was applied to save the measured results shown in Table 1, including start angle, end angle, and slipping distance.

From the results in Table 1, the crucial measurement factors, i.e., average value, standard deviation, and measurement uncertainty, were revealed.

The average value ($\overline{x}$) of the measurement is defined as

$$\overline{x} = \frac{1}{n}\sum_{i=1}^{n} x_i, \tag{3}$$

where x_i is the result of the ith measurement and n is the number of measurements.

The standard deviation (s) of the n measurements is defined as

$$s = \sqrt{\frac{\sum_{i=1}^{n}\left(x_i - \overline{x}\right)^2}{n-1}}. \tag{4}$$

Accordingly, the measurement uncertainty (u) is defined as

$$u = \frac{s}{\sqrt{n}}. \tag{5}$$

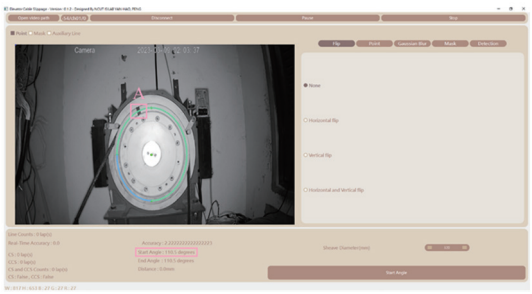

Fig. 28. (Color online) Location of start angle.

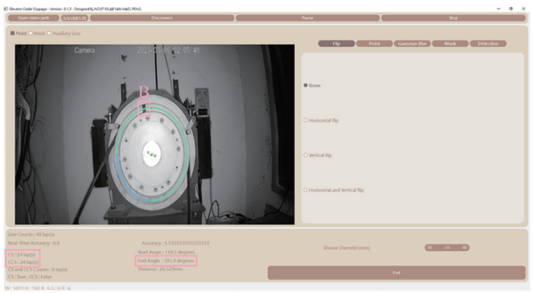

Fig. 29. (Color online) Location of end angle.

Table 1
Measurement results.

Test num.	Start angle	End angle	Slipping distance (mm)
1	90.5	81.0	26.529
2	81.0	71.0	27.925
3	71.0	62.0	25.133
4	52.5	42.5	27.925
5	42.5	33.0	26.529
6	33.0	24.0	25.133
7	24.0	14.0	27.925
8	14.0	5.0	25.133
9	342.0	333.0	25.133
10	322.5	313.0	26.529
11	313.0	303.0	27.925
12	303.0	293.0	27.925
13	293.0	283.0	27.925
14	283.0	273.5	26.529
15	273.5	264.5	25.133
16	264.5	255.5	25.133
17	255.5	246.0	26.529
18	216.5	206.5	27.925
19	206.5	197.0	26.529
20	197.0	187.5	26.529

Table 2
Results of measurement evaluation.

Item	Results (mm)
$\overline{x}$	26.599
s	1.153
u	0.258

The measurement data were substituted into Eqs. (2)–(4), and the results are shown in Table 2. As can be seen, the average slipping distance ($\overline{x}$) is 26.599 mm. More importantly, the standard deviation (s) is as low as 1.153 mm, and the measurement uncertainty (u) is only 0.258 mm. These values confirm that the proposed model can achieve a high measurement accuracy.

6. Conclusions

Elevator cable slippage is regarded as one of the most influential factors that may severely affect the safety of elevator operation. Presently, slippage detection is still mostly performed by visual inspection in industry today. To solve this problem, the streaming image process model for elevator cable slippage detection has been successfully demonstrated to achieve the following:

(1) The proposed model is insensitive to the position of wheel rotation. Here, only the wheel rotation start and end angles are needed to calculate the slipping distance by a simple arithmetic operation.
(2) The standard deviation (s) is as low as 1.153 mm, and the measurement uncertainty (u) is only 0.258 mm.
(3) The results obtained from elevator cable slippage measurement can be transmitted to the cloud instantly.
(4) The cable slipping status can be monitored online via web-based GUI soon after the slipping distance is calculated at every elevator operation.

Moreover, this proposed method can be applied to any type of elevator if the cable movement is pulled using a main wheel. The accuracy and precision when applied to other types of elevator will not be affected in practice owing to the model's insensitivity to the type of elevator.

Acknowledgments

This work was supported by the National Science and Technology Council, Taiwan (NSTC 112-2637-E-167-002).

References

1 P. Rizzo, E. Sorrivi, F. Scalea, and E. Viola: J. Sound Vibr. **307** (2007) 52. https://doi.org/10.1016/j.jsv.2007.06.058
2 C. Schaal, S. Bischoff, and L. Gaul: Struct. Health Monit. **15** (2016) 279. https://doi.org/10.1177/1475921716642747
3 F. Scalea, P. Rizzo, and F. Seible: J. Mater. Civ. Eng. **15** (2003) 219. https://doi.org/10.1061/(ASCE)0899-1561(2003)15:3(219)
4 X. Liu, B. Wu, F. Qin, C. He, and Q. Hanet: Ultrasonics **73** (2017) 196. https://doi.org/10.1016/j.ultras.2016.08.014
5 F. Ibáñez, A. Baltazar, and R. Mijarez: Smart Mater Struct. **24** (2015) 085036. https://doi.org/10.1088/0964-1726/24/8/085036
6 R. Raisutis, R. Kazys, L. Mazeika, V. Samaitis, and E. Zukauskas: Materials **9** (2016) 451. https://doi.org/10.3390/ma9060451
7 G. Zhang, Z. Tang, Y. Fan, J. Liu, H. Jahanshahi, and A. A. Aly: Sensors **21** (2021) 5401. https://doi.org/10.3390/s21165401
8 G. Zhang, Z. Tang, J. Zhang, and W. Gui: Sensors **20** (2020) 6612. https://doi.org/10.3390/s20226612
9 P. Zhou, G. Zhou, H. Wang, D. Wang, and Z. He: IEEE Trans. Instrum. Meas. **70** (2021) 1. https://doi.org/10.1109/TIM.2020.3011762
10 International ISO (the International Organization for Standardization) Standards, ISO 4101:1983, Technical Committee ISO/TC 105, Steel wire cables, September 1983.
11 P. Zhou, G. Zhou, and Z. He: Measurement **148** (2019) 106954. https://doi.org/10.1016/j.measurement.2019.106954
12 P. Zhou, G. Zhou, Y. Li, Z. He, and Y. Liu: IEEE Sens. J. **20** (2020) 8297. https://doi.org/10.1109/JSEN.2020.2970070

13 H. Shi, L. Zheng, S. Sun, L. Zhang, and L. Wang: J. Eng. **13** (2020) 517. https://doi.org/10.1049/joe.2019.1152
14 D. H. Yang, K. Y. Kim, M. K. Kwak, and S. Lee: J. Soun. Vibr. **390** (2017) 164. https://doi.org/10.1016/j.jsv.2016.10.045
15 J. Bao, P. Zhang, C. Zhu, and M. Zhu: Inter. J. Soun. Vibr. **20** (2015) 160. https://doi.org/10.20855/ijav.2015.20.3380
16 J. Bao, P. Zhang, C. Zhu, and W. Sun: J. Mech. Sci. Technol. **28** (2014) 457. https://doi.org/10.1007/s12206-013-1110-y
17 T. X. Nguyen, N. Miura, and A. Sone: Earthquake Eng. Eng. Vibr. **18** (2019) 447. https://doi.org/10.1007/s11803-019-0514-9
18 M. Otsuki, K. Yoshida, S. Nakagaki, T. Nakagawa, S. Fujimoto, and H. Kimura: Proc. Inst. Mech. Eng., Part I: J. Syst. Control Eng. **218** (2004) 531. https://doi.org/10.1177/095965180421800702
19 N. Miura, T. Matsuda, Y. Higashi, H. Ono, and X. T. Nguyen: J. Asian Archit. Build. Eng. **22** (2023) 1533. https://doi.org/10.1080/13467581.2022.2086876
20 M. Benosman: IEEE Trans. Control Syst. Technol. **22** (2014) 1855. https://doi.org/10.1109/TCST.2013.2294094
21 D. H. Yang, K. Y. Kim, M. K. Kwak, and S. Lee: J. Soun. Vibr. **390** (2017) 164. https://doi.org/10.1016/j.jsv.2016.10.045
22 Q. Zhang, Y. Yang, T. Hou, and R. Zhang: Noise Vibr. Worldwide **50** (2019) 37. https://doi.org/10.1177/0957456519827929
23 J. Rostami, P. W. Tse, and M. Yuan: Struct. Health Monit. **19** (2020) 481. https://doi.org/10.1177/1475921719855915
24 Y. Kou, J. Guo, J. Li, S. Jiao, J. Liu, Z. Yan, and K. Zhu: IEEE Access **10** (2022) 63619. https://doi.org/10.1109/ACCESS.2022.3183097
25 Q. Zhen, Y. Wu, J. Cong, and S. K. Lyu: Machines **10** (2022) 1180. https://doi.org/10.3390/machines10121180
26 H. Lin and Y. Peng: Proc. 2023 The 8th IEEE/ACIS Int. Conf. Big Data, Cloud Computing, and Data Science (IEEE, 2023) (in press).